In Situ Synthesis of MXene with Tunable Morphology by Electrochemical Etching of MAX Phase Prepared in Molten Salt

Liyuan Liu, Hannes Zschiesche, Markus Antonietti, Mathieu Gibilaro, Pierre Chamelot, Laurent Massot, Patrick Rozier, Pierre-louis Taberna, Patrice Simon

ADVANCED ENERGY MATERIALS
www.advenergymat.de

In Situ Synthesis of MXene with Tunable Morphology by Electrochemical Etching of MAX Phase Prepared in Molten Salt

Liyuan Liu, Hannes Zschiesche, Markus Antonietti, Mathieu Gibilaro, Pierre Chamelot, Laurent Massot, Patrick Rozier, Pierre-Louis Taberna, and Patrice Simon**

MXenes, a rapidly growing family of 2D transition metal carbides, carbonitrides, and nitrides, are one of the most promising high-rate electrode materials for energy storage. Despite the significant progress achieved, the MXene synthesis process is still burdensome, involving several procedures including preparation of MAX, etching of MAX to MXene, and delamination. Here, a one-pot molten salt electrochemical etching (E) method is proposed to achieve Ti_2C MXene directly from elemental substances (Ti, Al, and C), which greatly simplifies the preparation process. In this work, different carbon sources, such as carbon nanotubes (CNT) and reduced graphene oxide (rGO), are reacted with Ti and Al micro-powders to prepare Ti_2AlC MAX with 1D and 2D tuned morphology followed by in situ electrochemical etching from Ti_2AlC MAX to Ti_2CT_x MXene in low-cost LiCl-KCl. The introduction of the O surface group via further ammonium persulfate (APS) treatment can act in concert with Cl termination to activate the pseudocapacitive redox reaction of $Ti_2CCl_yO_z$ in the non-aqueous electrolyte, resulting in a Li^+ storage capacity of up to 857 C g^{-1} (240 mAh g^{-1}) with a high rate (86 mAh g^{-1} at 120 C) capability, which makes it promising for use as an anode material for fast-charging batteries or hybrid devices in a non-aqueous energy storage application.

1. Introduction

Early transition metal carbides and nitrides (MXenes) are an essential class of 2D materials owing to their high hardness, hydrophilic surfaces, and high metallic conductivity.[1–4] With a general formula of $M_{n+1}X_nT_x$ (n = 1–3), MXenes are commonly prepared by selective etching of the atomically thin A layer elements from MAX phase precursors, where M represents an early transition metal, A stands for an element from group 13–16, X is carbon and/or nitrogen, and T represents the surface groups originating from the etching procedure.[5] Over the last decade, hazardous HF solutions were mainly used as the etchant, which inevitably poses safety concerns and limits the scalable preparation.[4,6] In addition, the conventional HF-etching preparation method of MXene limits the surface of functional groups to −F, −OH, and −O, which is a clear bottleneck for optimizing their electrochemical properties.[7] Accordingly, efforts aimed to discover environmental-friendly F-free synthesis routes over-controlled surface termination, are in progress worldwide.

Recently, a general molten salt synthetic route was reported to prepare MXenes (termed as MS-MXene) by using Lewis acidic melts ($ZnCl_2$, $CuCl_2$, etc.) for etching MAX. Interestingly, by playing with the wide range of elements for the A-site of the MAX precursors (Zn, Al, Si, Ga) and the Lewis acid melt composition, this method broadens the choice of MAX-phase families for MXene fabrication with great opportunities to tune their surface chemistries.[7] The as-prepared Cl and O-terminated MXene used as a negative electrode in Li-ion-containing electrolyte could deliver a capacity of about 200 mAh g^{-1} at a 1 C rate. Unfortunately, the whole process is time-consuming and complicated, which involves the preparation of MAX, the etching of MAX to MXene, and the

L. Liu, P. Rozier, P.-L. Taberna, P. Simon
CIRIMAT
UMR CNRS 5085
Université Paul Sabatier Toulouse III
118 route de Narbonne, 31062 Toulouse, France
E-mail: pierre-louis.taberna@univ-tlse3.fr; patrice.simon@univ-tlse3.fr

The ORCID identification number(s) for the author(s) of this article can be found under https://doi.org/10.1002/aenm.202203805.

DOI: 10.1002/aenm.202203805

L. Liu, P. Rozier, P.-L. Taberna, P. Simon
RS2E
Réseau Français sur le Stockage Electrochimique de l'Energie
FR CNRS 3459, 80039 Amiens Cedex, France

H. Zschiesche, M. Antonietti
Max Planck Institute of Colloids and Interfaces
Research Campus Golm
D-14476 Potsdam, Germany

M. Gibilaro, P. Chamelot, L. Massot
Laboratoire de Génie Chimique
Université Paul Sabatier Toulouse III
UPS-CNRS-INPT
118 Route de Narbonne, 31062 Toulouse Cedex 9, France

removal of metal impurities. To further shorten the synthesis duration, Lin et al.[8] proposed the Ti_2CT_x synthesis in the air via the formation of Ti_2AlC followed by adding $CuCl_2$ etchant in one molten salt pot, which requires adding the Lewis acidic salt by opening the furnace door at 700 °C, thus bringing safety risk. More importantly, it still requires an oxidative washing treatment to remove the metal impurities formed during the synthesis by reducing the metal cation (Cu^{2+} for instance), inevitably leaving many O surface groups on MXene. In addition, although the researchers are excited about the electrochemical performance of MS-MXene with halogen-containing surface groups in non-aqueous electrolytes[6–8] over the past two years, the contribution of the halogen surface groups to the electrochemical behavior is still to be understood.

Following these previous works, a molten-salt-assisted electrochemical etching method was adopted to synthesize $Ti_3C_2Cl_2$ from commercial Ti_3AlC_2 without introducing any metallic impurities.[9] However, similar to the other electrochemical etching methods to prepare MXene in aqueous electrolytes, such as TMAOH,[10] LiOH/LiCl,[11] and HCl,[12] this method uses expensive commercial MAX phase precursors, and as a consequence, the morphology and texture of the prepared MXenes are derived from the ones of the MAX precursors. Over the last decade, researchers have spent a lot of effort studying the etchant and etching process from MAX to MXene,[13] while ignoring the challenges and opportunities in tailoring MAX phases as a starting material for MXenes development.[14,15]

In this work, using carbon nanotube (CNT) and reduced graphene oxide (rGO) as carbon source, Ti_2AlC with 2D and 1D morphologies were prepared, followed by an in situ molten salt electrochemical etching to prepare Ti_2CT_x MXene. Then, an oxidative chemical treatment by immersion in ammonium persulfate (APS) solution is performed to introduce large amounts of O-containing terminations onto the MXene surface and then to distinguish the impact of the halogen Cl versus O surface terminations onto its electrochemical performance. Electrochemical characterizations of these APS-treated E-$Ti_2CCl_yO_z$ in 1 M $LiPF_6$ carbonate-based electrolyte have revealed high charge–discharge rate capability and pseudocapacitive-like electrochemical signature, offering exciting opportunities as high-power electrodes for energy storage devices.

2. Results and Discussion

2.1. Synthesis of E-Ti_2CT_x

Figure 1a shows a sketch of the molten salt cell, where a pellet made of stoichiometric amounts of titanium (Ti), aluminum (Al), and carbon (C) powders were used as the working electrode with molten salt crucible as a counter electrode, and a glassy carbon rod as a quasi-reference electrode, respectively. Using CNT and rGO as carbon sources, respectively, Ti_2AlC MAX with 1D and 2D tuned morphology can be prepared in the first annealing step at 950 °C while a following in situ electrochemical etching step is performed at 500 °C to achieve one pot etching of Ti_2AlC MAX to Ti_2CT_x MXene (Figure 1a).

Prior to the insertion of the working electrode, the electrochemical cell containing the mixture of LiCl and KCl (T_m = 354 °C) is heated up to 950 °C, where the salt transforms into a liquid phase with high-temperature stability, low viscosity, and high ion mobility.[16] The reaction process starts

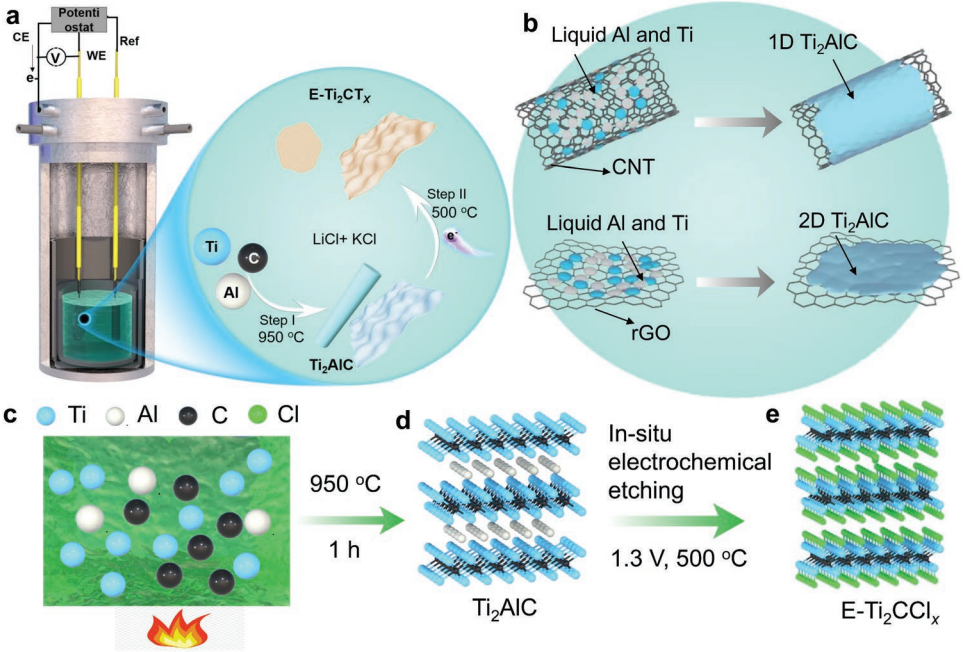

Figure 1. Schematic illustration of the fabrication process of Ti_2AlC and E-Ti_2CT_x. a) The schematics of the molten salt cell with the (Ti, Al, C) pellet used as the working electrode, glass carbon as the reference electrode with the graphite crucible used as the counter electrode. b) The reaction scheme of 1D and 2D Ti_2AlC production using CNT and rGO as carbon sources. c) The (Ti, Al, C) pellet immersed in LiCl/KCl molten salt is heated at 950 °C for 1 h to d) prepare the Ti_2AlC MAX phase, followed by e) an electrochemical etching at 1.3 V for 24 h to obtain the E-Ti_2CCl_x MXene.

once the pellet is introduced inside the molten salt cell. Previous work using graphite as the carbon source suggested the formation of Ti-Al alloy on the titanium surface when titanium (melting point 1668 °C) was surrounded with melted aluminum (melting point 660 °C) at elevated temperatures, while TiC was grown on the graphite side.[17] Combined with the further increased temperature, Ti_2AlC nucleation occurs at the expense of Ti-Al intermetallic and TiC species, giving rise to the formation of Ti_2AlC grains (Equation (1), Figure 1b). Carbon has the highest melting point of 3550 °C[18] and lowest solubility, thus offering the possibility of using carbon as a structural skeleton and template for MAX phase preparation.[15] Here, CNT or rGO is used as a carbon source, with the expectation of 1D or 2D MAX phase preparation as illustrated in Figure 1b.

$$Ti + Al + C \xrightarrow{LiCl/KCl} Ti_2AlC \quad (1)$$

As schematically shown in Figure 1c,d, thanks to the rapid diffusion of reactants in the molten salt flux,[19] the Ti_2AlC MAX particles synthesis can be achieved at 950 °C in 1 h, which requires lower temperature and shorter reaction time compared to most of the reported methods such as the pressure-less sintering, spark plasma sintering, or other molten salt methods.[20]

In a second step to achieve one-pot preparation of MXene via an electrochemical etching, the molten salt cell is cooled down to 500 °C and connected to a potentiostat in a three-electrode set-up where the pellet is used as a working electrode, the stainless-steel vessel in contact with molten salt crucible as a counter electrode, and a glassy carbon rod immersed inside the molten salt is taken as a quasi-reference electrode, respectively (see Figure 1a). Indeed, the stronger bonding of M-X versus M-A atoms[21] offers the opportunity to selectively etch the A layer out of the MAX phase without breaking M-X bonds. A controlled positive voltage was then applied to selectively remove Al atoms from the MAX phases at low voltage (1.3 V versus ref.), to avoid Ti etching that was observed at high polarization, resulting in the formation of carbide carbon atoms (CDC).[22] At a constant voltage of 1.3 V versus ref. (Figure 1d,e), the following etching mechanism is assumed: the Al-atoms are oxidized into Al^{3+} and deintercalated from the Ti_2AlC phase; the Al^{3+} ions in the LiCl/KCl molten salt then form a volatile $AlCl_3$ phase (Equation (2)) while the free Cl^- from the molten salt fills the vacancy of the Ti_2C to form the surface terminal group −Cl (Equation (3)).[7] At the same time, free Li^+/ K^+ ions in the molten salt move to the negative electrode, where they are reduced forming a Li/K metal deposit (Equation (4)).[9]

The electrochemical etching processes at the anode (positive electrode) are (Equations (2) and (3))

$$3Cl^- + Ti_2AlC \xrightarrow{LiCl/KCl} Ti_2C + AlCl_3(g)\uparrow + 3e^- \quad (2)$$

$$Ti_2C + xCl^- \xrightarrow{LiCl/KCl} E - Ti_2CCl_x + xe^- \quad (3)$$

At the counter electrode (negative electrode), the following cathodic reaction occurs

$$Li^+(K^+) + e^- \xrightarrow{LiCl/KCl} Li(K) \quad (4)$$

2.2. Material Characterization of Ti_2AlC and E-Ti_2CCl_x

Figure S1, Supporting Information, shows the X-ray diffraction (XRD) patterns of Ti, Al, and C stoichiometric mix powders heated in LiCl/KCl flux at various temperatures after various reaction times. The target phase Ti_2AlC is present at 900 °C, mixed with sub-stoichiometric TiAl, $TiAl_2$, and TiC. As the annealing temperature is increased to 950 °C and the reaction time extended to 1 h, the content of the target phase grows and Ti_2AlC was synthesized successfully after 1 h. XRD patterns and Rietveld refinement of the Ti_2AlC MAX phase (space group of P 6_3/mmc) are shown in Figure S2, Supporting Information, with lattice parameters of a = 0.306 nm and c = 1.365 nm, while some traces of TiC (≈8 wt%) are detected. Further increasing the dwell time and dwell temperature to 3 h at 1100 °C results in the decomposition and transformation of Ti_2AlC into TiC, which is induced by carbothermal reduction promoted by the use of excess C and large amounts of molten salt flux.[16]

In a second step, the molten salt cell was cooled down to 500 °C and MXene was prepared from the MAX phase by electrochemical etching at a constant potential, where the positive electrode (Ti_2AlC) is oxidized to remove the Al; the applied voltage then plays a vital role in the final product. The XRD crystal structure patterns after constant-voltage etching at different voltages are displayed in Figure S3, Supporting Information. When the voltage is lower than 0.5 V versus ref., the Ti_2AlC remains, revealing that Al atoms cannot be oxidized at such low voltage. As the applied voltage is increased to 1.3 V versus ref., for an etching period of 18 h, the MXene displays a noticeable shift of (002) peak from 13° to 10.5°, corresponding to an enlarged d-spacing (8.4 Å) than the pristine Ti_2AlC (6.7 Å). Such a d-spacing change indicates effective electrochemical-etching[7,9] (termed as E-etching). However, under these conditions, some residue of Ti_2AlC precursors is inevitably retained in the E-etched MXenes. When the etching period is extended from 18 to 24 h, the current during the etching process using 1.3 V versus Ref. is around 3.6 Å (Figure S4, Supporting Information), and all the diffraction peaks of Ti_2AlC MAX disappear, thus evidencing the complete etching of Ti_2AlC phase into E-Ti_2CCl_x. In addition, EDS analysis (Figure S5, Supporting Information) shows a drastic decrease of the Al content from 28% for pristine Ti_2AlC down to 0.75% for the sample collected after the E-etching process confirming the successful etching of Al to prepare E-Ti_2CCl_x—those results are in line with the etching process mechanism proposed. Moreover, Ti_2CT_x MXene is also prepared by conventional etching of commercial Ti_2AlC in $CuCl_2$ -containing molten salt,[7] its XRD pattern in Figure S6, Supporting Information, shows that the (002) peak position is also located at 10.5°, which further validates that molten salt electrochemical etching method is efficient to prepare MXene. In addition to etching time, Ti_2AlC samples are also etched at higher voltages (Figure S7, Supporting Information). When the voltage is set as 2 V versus ref. and etched for 24 h, the TiC single phase is observed, suggesting the excessive oxidation leading to a full etching of Ti from Ti_2AlC at high voltage, in agreement with previous work which reported the full etching of Al and Ti at high voltage, to make carbide-derived carbon atoms (CDC).[22]

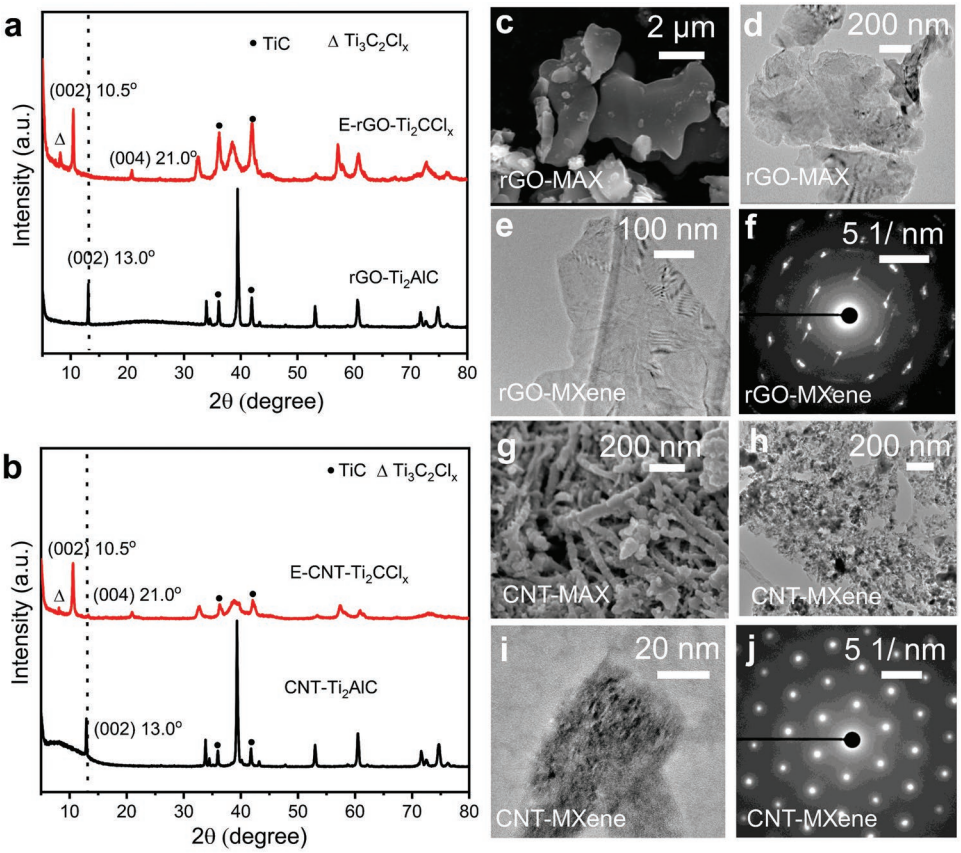

Figure 2. Characterizations of Ti_2AlC MAX phase and E-Ti_2CCl_x MXene prepared using 2D (rGO) and 1D (CNT) carbon sources. XRD patterns of a) rGO and b) CNT-based MAX and MXene. rGO-Ti_2AlC MAX: c) SEM and d) TEM images; E-rGO-Ti_2CCl_x MXene: e) TEM image and f) SAED pattern; CNT-Ti_2AlC MAX phase: g) SEM images at a scale of 200 nm; E-CNT-Ti_2CCl_x MXene: TEM image at a scale of h) 200 nm and i) 20 nm, and j) SAED pattern.

Then, the influence of the carbon precursor morphology was studied. For that purpose, two different carbons, including rGO and CNT, were used as carbon sources. The as-prepared Ti_2AlC MAX and Ti_2CT_x MXene from rGO are denoted as rGO-Ti_2AlC and E-rGO-Ti_2CCl_x; in the same way, the as-prepared Ti_2AlC MAX and Ti_2CT_x MXene from CNT are termed as CNT-Ti_2AlC and E-CNT-Ti_2CCl_x. rGO-based MAX and MXene (**Figure 2**a) show similar XRD patterns as the CNT-based MAX and MXene (Figure 2b), both exhibiting sharp diffraction peaks, suggesting high crystallinity. However, a small peak at 8° can be observed in E-Ti_2CCl_x, implying the formation of the $Ti_3C_2Cl_x$ phase. This might be explained by the partial transformation of Ti_2AlC into Ti_3AlC_2 already reported to easily occur during the annealing process.[23] In addition, Figure 2a shows a higher intensity of Bragg peaks at 36° and 41.8°, which may indicate more formation of TiC phase using rGO than using CNT as the result of the higher redox reactivity of rGO than CNT due to its rich functional groups.[24] As shown in Figure 2c, a typical scanning electron microscope (SEM) image reveals that the as-grown rGO-Ti_2AlC grains are composed of 2D flakes with a lateral size of about 5 μm, which retained the morphologies of the as-received rGO flakes. Furthermore, the transparency of the flakes as observed in the transmission electron microscopy (TEM) image (Figure 2d) evidences its small thickness. The sample thickness is measured by high-resolution TEM (HRTEM) to about 6.5 nm (Figure S8a, Supporting Information), corresponding to ≈10 layers, considering the thickness of a monolayer (0.67 nm). After electrochemical etching, the E-rGO-Ti_2CCl_x sheets (Figure 2e) appear transparent with a well-defined and clean edge morphology—with a lateral size of around 700 nm. The HRTEM image in Figure S8b, Supporting Information, confirms a thickness of about 1.82 nm, corresponding to ≈2 layers considering the thickness of the monolayer (≈0.88 nm). The regular diffraction spots (Figure 2f), as shown in the selected area electron diffraction (SAED) pattern, evidence the basal hexagonal symmetric structure and high crystallinity of E-rGO-Ti_2CCl_x, indicating that the original rGO-Ti_2AlC structure is still maintained after etching. The high-resolution SEM image in Figure 2g shows that it exhibits 1D nanorod morphology with a diameter of around 50 nm. Instead of the hollow CNT morphology from the carbon source, the cross-section of CNT-Ti_2AlC after focused ion beam (FIB) treatment (Figure S9, Supporting Information) shows a bulk nanorod morphology, as a result of the MAX growth mechanism. After electrochemical etching, the nanorod broke down into very small particles in large aggregation (Figure 2h). The HRTEM image in Figure 2i shows that the E-CNT-Ti_2CCl_x are tiny particles (Figure 2i) with a lateral size of ≈30 nm, which owns the similar shape of a cross-section from nanorod MAX phase as shown in Figure S9, Supporting Information. Its

crystallinity is evidenced by the SAED pattern and the sharp reflections indexed with a hexagonal crystal system (Figure 2j).

The above CNT-Ti_2CCl_x and rGO-Ti_2CCl_x, obtained from different carbon precursors, show significantly different morphology from the conventional accordion-like morphology prepared by etching commercial Ti_2AlC particles of tens of microns in Lewis acidic $CuCl_2$ (Figure S10, Supporting Information). In addition, different carbon source, such as graphite, was also mixed with Ti and Al powders to prepare Ti_2AlC MAX, resulting in aggregated dense bulky grains (see Figure S11, Supporting Information) with a mean length of 50 µm. The above different morphologies of Ti_2AlC MAX were similar to that of the as-used carbon sources, revealing that the formation of Ti_2AlC MAX can be tuned by the carbon morphology. This can be explained by the difference in the solubility of Ti and Al in the molten salt itself directly related to their respective melting temperature (1668 °C for Ti and 660 °C for Al) compared to carbon (3550 °C). TiAl and TiC are formed, and the MAX phase synthesis reaction starts from the surface of the carbon.[17]

The atomic and electronic structure of the as-prepared Ti_2AlC were characterized using HR scanning transmission electron microscopy (STEM). Layers of ordered Ti_2AlC MAX are resolved in a cross-sectional view along basal planes in **Figure 3**a and even resolving atomic columns in Figure 3b. The periodicity measured from the HR-STEM image is 0.67 nm along the (0001) direction, well matching with the (00l) peak in the XRD pattern as displayed in Figure 2a. As shown in the High-angle annular dark-field (HAADF)-STEM and its related intensity line profile (see Figure 3a,b), up to two bright and one dark atomic planes can be identified per Ti_2AlC MAX layer. This bright contrast is directly interpretable as a mass (atomic number)-thickness contrast.[3,4] Combined with the EDS analysis acquired by scanning over the local cross-section region (Figure S12, Supporting Information), assuming a homogeneous thickness, the inner bright planes can be related to atomic planes occupied by Ti and the outer dark planes to A sites mainly occupied by Al. Same as per the previous report,[8] no signal of C was detected within the Ti_2C structure in HAADF-STEM imaging due to its small atomic number. As shown in Figure 3b, the centered brighter planes marked by blue spheres represent Ti atoms, while the dark planes marked by white spheres indicate Al atoms. Every two bright atomic planes are separated by one dark atomic plane, further confirming the Ti_2AlC crystal structure as displayed in Figure 3b. The atomic structure of E-rGO-Ti_2CCl_x has also been resolved by HR-STEM and local electron energy loss spectroscopy (EELS). Combining the EELS mapping results showing that Cl and Ti layers alternate (Figure 3c), the inner brighter planes can be attributed to atomic planes of Ti, while the outer bright planes with a lower brightness are associated with atomic planes of Cl surface terminations, positioned on top or bottom of the neighboring Ti atomic planes. However, there are three bright Ti layers in the middle while the top and bottom one only shows two bright Ti layers, indicating the appearance of $Ti_3C_2Cl_x$ phase composition sandwiched by the Ti_2CCl_x phase, which agrees well with the previous XRD result (Figure 2a), further evidencing the partial transformation of Ti_2AlC into Ti_3AlC_2 during the synthesis (950 °C) or the electrochemical etching procedure (500 °C).

Furthermore, EELS is particularly suitable for the study of light elements and transition metals (O, C, Cl, Ti), thus can

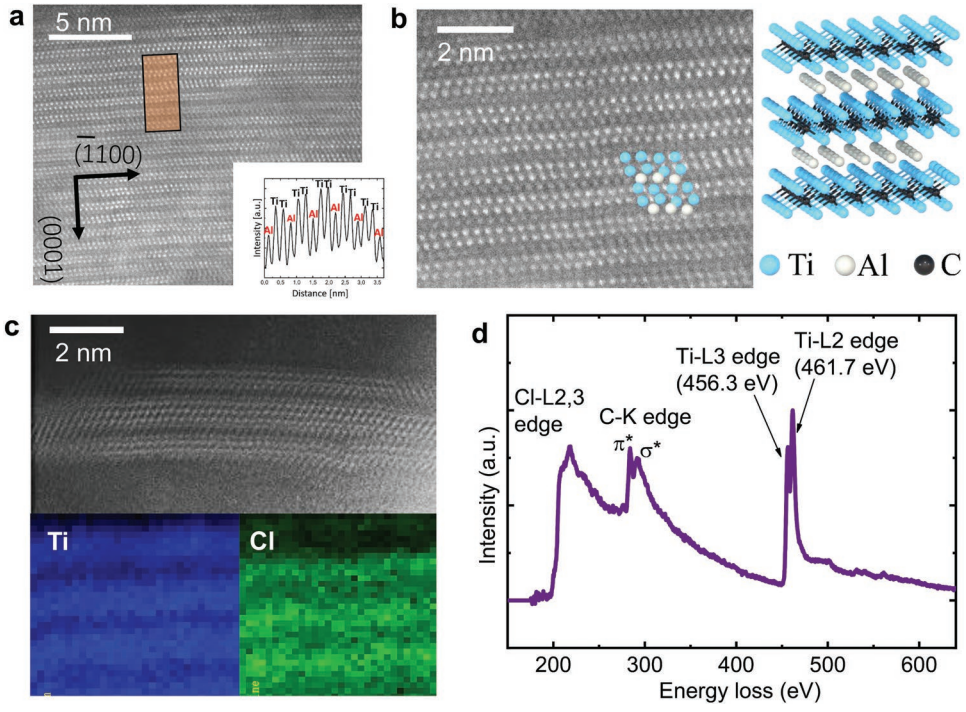

Figure 3. Atomic and electric structural analysis of rGO-Ti_2AlC and E-rGO-Ti_2CCl_x. Atomic resolution high-angle annular dark-field (HAADF) images of rGO-Ti_2AlC at a scale of a) 5 nm and its corresponding intensity line profile; b) HAADF image of rGO-Ti_2AlC at a scale of 2 nm with an inset of the corresponding crystal structures. c) HAADF image of E-rGO-Ti_2CCl_x at a scale of 2 nm and its atomic-scale electron energy-loss spectroscopy (EELS) mapping. d) EELS analysis of E-rGO-Ti_2CCl_x.

be used to investigate the T-groups desorption by focusing on the Cl-L2,3 edges on the nanometer scale. In comparison to the EELS result of $FeCl_2$ etched followed by magnet-treated $Ti_3C_2Cl_x$ (Figure S13, Supporting Information), E-rGO-Ti_2CCl_x has Cl-L2,3, C-K, and Ti L2,3 edges at similar positions (approximate peak maximum) of ≈208, ≈217, 284, and 293 eV and ≈456 and ≈462 eV energy loss, respectively. The C-K edge of Cl-containing $Ti_3C_2Cl_x$ shows the peaks at ≈283.8 and ≈292.8 eV characteristic of sp2 carbon atoms in a hexagonal structure, attributed to transitions from an initial 1s state to unoccupied antibonding-like π^* and σ^* states above the Fermi level.[25] However, the different "fine structure" of C edges and π^* and σ^* ratio variation with higher σ^* ratio is also observed as shown in Figure S14, Supporting Information, indicating the existence of "surrounding" phases amorphous C phase in some areas.[26] In addition, E-rGO-Ti_2CCl_x does not show an obvious O edge as $FeCl_2$ etched $Ti_3C_2Cl_x$, suggesting the lower O content after electrochemical etching.

2.3. Electrochemical Characterizations

In previous reports,[6–8] we showed that Cl- and O-terminated MXene could achieve a reversible fast Li-ion intercalation when used as a negative electrode in non-aqueous electrolytes. However, the APS ($(NH_4)_2S_2O_8$) washing step not only removed Cu but also resulted in an increased content of O-surface terminations due to partial MXene oxidation, making it difficult to distinguish the impact of halogen Cl versus O-containing surface terminations onto its electrochemical performance.[7] To do so, the O-free, Cl-terminated E-Ti_2CCl_x were treated by APS, and a series of material and electrochemical characterizations were performed to compare their electrochemical performance before and after APS treatment. As shown in the XRD patterns of Figure S15, Supporting Information, while the peak position remains the same, the peak at 8° shows a higher intensity, indicating more Ti_3C_2-based MXene phase got exposed after APS treatment. In addition, Fourier-transform infrared spectroscopy (FTIR) results (Figure S16, Supporting Information) show the appearance of C=O and Ti—O surface group after APS treatment, which is consistent with the TPD-MS results showing the formation of CO_2 gas and XPS analysis showing the formation of C—Ti—O bonding,[27] and a partial exchange of Cl with oxygen-containing functional groups. Washing in APS ($(NH_4)_2S_2O_8$) then results in the transformation of Cl-terminated E-Ti_2CCl_x to Cl and O-terminated E-$Ti_2CCl_yO_z$.

A series of electrochemical characterizations were performed in 1 M $LiPF_6$/ethylene carbonate-dimethyl carbonate electrolyte (LP30) to evaluate the electrochemical performance of E-CNT-Ti_2CT_x before and after APS treatment. The cyclic voltammetry (CV) profiles displayed in **Figure 4**a were recorded from 0.01 to 3 V versus Li^+/Li at a scan rate of 0.5 mV s^{-1}. While Cl-terminated E-CNT-Ti_2CCl_x before APS treatment exhibits a low current density within the whole voltage window, the APS-treated E-CNT-$Ti_2CCl_yO_z$ shows a more symmetric and mirror-like CV profile, with no redox peaks during (de)intercalation of Li-ions, revealing a typical intercalation pseudocapacitive electrochemical signature[28,29] associated with the fast electrochemical kinetic reaction. This finding shows that the Li capacity is highly likely dependent on the presence of oxygen-containing functional groups.

A comparison of the specific capacity change with discharge time (Figure 4b) of the E-CNT-Ti_2CT_x and E-rGO-Ti_2CT_x samples before and after APS treatment calculated from CV and galvanostatic tests (Figures S17 and S18 and Table S1, Supporting Information), further confirms the higher specific capacities of the APS treated E-$Ti_2CCl_yO_z$ electrode. Similar weight loadings of 1.5 mg cm^{-2} are used for both materials so the slower kinetics may be assigned to the lower content of the O-containing functional group of E-CNT-Ti_2CCl_x. The discharge capacity of APS-treated E-CNT-$Ti_2CCl_yO_z$ reaches 240 mA h g^{-1} at a scan rate of 0.5 mV s^{-1} ≈100 min discharge time (0.6 C rate) and 86 mA h g^{-1} at a scan rate of 100 mV s^{-1} ≈0.5 min discharge time (120 C rate), corresponding to a capacity retention of 36%, highlighting its high-power capability. Comparatively, the discharge capacities of pristine E-CNT-Ti_2CCl_x can only reach 151 and 22 mA h g^{-1} at the same scan rates of 0.5 and 100 mV s^{-1}, respectively, which corresponds to a capacity retention of only 14%. Similarly, the introduction of O content, thanks to the APS treatment, increases the capacity of APS-treated E-rGO-MXenes but the capacity and power capability were found to be lower than the E-CNT-MXenes (Figure 4b). Such performance decrease for E-rGO-MXenes might be explained by its larger size (Figure 2e) and the presence of more TiC impurities (Figure 2a,b), suggesting the effectiveness of improving the electrochemical properties by tuning the morphology.[30,31] Since E-CNT-$Ti_2CCl_yO_z$ shows a higher capacity and better power capability, it has been selected for further electrochemical characterization.

Figure 4c presents the charge/discharge voltage profiles of the E-CNT-$Ti_2CCl_yO_z$ electrode from galvanostatic tests at different C-rates, which confirm the unique electrochemical signature with a sloping voltage profile within the potential range of 0.01–1.8 V versus Li^+/Li, as expected from the cyclic voltammetry profiles (Figure 4a). As the specific current increases, discharge capacities of 253 and 135 mAh g^{-1} could be delivered at specific currents of 0.1 and 2 A g^{-1}, which further evidences the high-power capability for our E-CNT-$Ti_2CCl_yO_z$ electrode. Figure S20, Supporting Information, shows a capacity retention of 81% after 2000 cycles at 2 A g^{-1}. Electrochemical impedance spectroscopy (EIS) measurements were also performed at various biased voltages for the E-CNT-$Ti_2CCl_yO_z$ electrode to understand the reaction process thoroughly. Figure 4d shows the Nyquist plots recorded at various constant potentials during discharge (reduction). While the Nyquist plot reveals a blocking-like electrochemical behavior at 2.5 V as the result of the absence of intercalation reaction, the high-frequency loop appearing when decreasing the potential is associated with the charge transfer process corresponding to the Li-ion intercalation reaction in the MXene electrodes, together with the formation of the solid electrolyte interphase (SEI) film. As expected, the charge transfer resistance slightly decreases when increasing the cathodic overpotential, and the rapid increase in the imaginary part of the impedance at low frequency highlights the fast (pseudocapacitive) Li-ion intercalation reaction.[8]

Thanks to the design of a specific MXene synthesis via molten salt electrochemical etching without metal impurity, it is now possible to distinguish experimentally between the

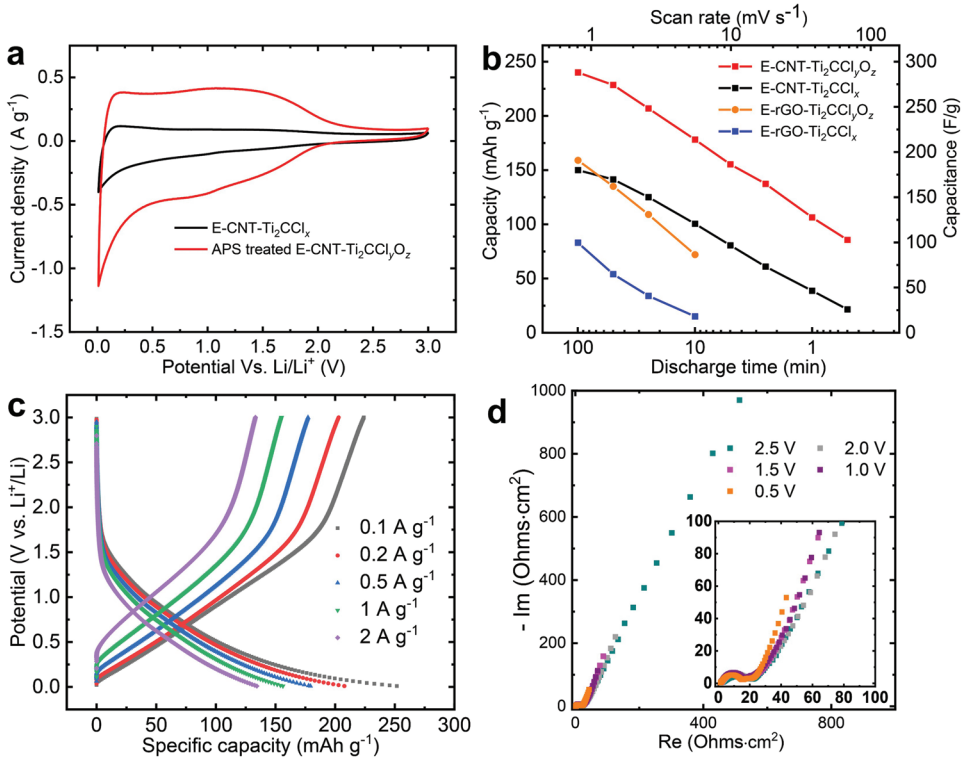

Figure 4. Electrochemical characterization of E-Ti_2CT_x before and after APS treatment. a) Comparison of the CV plots of E-CNT-Ti_2CT_x before and after APS treatment recorded at a potential scan rate of 0.5 mV s^{-1}, b) Comparison of the specific capacity and capacitance at various scan rates of E-CNT-Ti_2CT_x and E-rGO-Ti_2CT_x before and after APS treatment, c) Galvanostatic charge/discharge profiles and d) electrochemical impedance measurements at various potentials of the E-CNT-Ti_2CT_x after APS treatment.

contributions of Cl- and O-surface termination groups by comparing MXene's electrochemical behavior before and after APS treatment. The results show that the presence of oxygen-containing functional groups activates the electrochemical Li intercalation redox reaction in E-CNT-$Ti_2CCl_yO_z$ in the LP30 electrolyte. This experimental finding agrees with previous modeling results,[32] reporting that O-containing functional groups of MXenes are active sites for Li^+ to boost the lithium storage performance. Specifically, DFT calculations have shown that the Li-ion migration barrier[33] and adsorption energies[32] could be greatly decreased after partial O substitution, resulting in the rapid diffusion of Li-ions and strong interaction between O and Li-ions. Therefore, a high Li-ion storage capacity can be achieved with O-terminated MXene thanks to the adsorption of more Li ions. Similarly, improved Li-ion capacity has been observed after increasing the O content by annealing HF-$Ti_3C_2T_x$ under an Ar atmosphere.[33] However, the lithium intercalation/deintercalation reaction in F- and O-terminated HF-$Ti_3C_2T_x$ occurs within a broad voltage window of 0.05 V up to 3 V versus Li^+/Li.[33] Such a large operating potential window range—resulting in a high average operating potential for a negative electrode—together with extremely slow intercalation kinetics (50% capacity loss between 1 and 8 C rate)[34] drastically limits the interest of such MXene materials for Li-ion battery applications. Differently, the Li intercalation process in Cl- and O-terminated $Ti_2CCl_yO_z$ MXene prepared from 1D MAX phase could be achieved in a continuous way without redox peaks within a narrow potential window (≈0.01 V up to 1.8 V vs Li^+/Li) compared to HF-MXenes. Moreover, the excellent rate capability of 86 mAh g^{-1} at 120 C rate makes E-CNT-$Ti_2CCl_yO_z$ a great candidate as an anode for high-rate Li-ion batteries. In summary, we can conclude that Cl- and O-termination of E-CNT-$Ti_2CCl_yO_z$ act in concert to enable high Li-ion storage capability at a high rate, while unitary Cl-terminated E-CNT-Ti_2CCl_x shows poor electrochemical performance. These results provide an understanding of the effect of surface terminations on the electrochemical properties of MS-MXenes.

3. Conclusions

In this study, we proposed a simple one-pot electrochemical etching approach to preparing Cl-terminated Ti_2C MXene (Ti_2CCl_x) directly from Ti, Al, and C powders in low-cost molten salts LiCl/KCl. By using different carbon sources with different morphologies, such as CNT and rGO, MAX and MXene with tuned morphology could be prepared based on the "carbon-template-growth" mechanism, providing another pathway for further control over their properties. The electrochemical redox reaction of E-Ti_2CT_x MXene could be activated by the introduction of the O-containing functional group via APS washing. When used as an anode material for nonaqueous Li-ion storage, the obtained E-CNT-$Ti_2CCl_yO_z$ MXene exhibits a lithiation capacity of ≈240 mAh^{-1} at 0.6 C rate and 86 mAh g^{-1} could still be delivered at a high charge/discharge rate of 120 C. Those results show that tuning the surface chemistry of MXene

is of key importance for enhancing their electrochemical properties, providing guidelines for preparing a new generation of MXene negative electrodes for high-power batteries.

4. Experimental Section

Preparation of LiCl-KCl Molten Salt Bath: Anhydrous LiCl (99% purity, Sigma Aldrich) and KCl (99% purity, Sigma Aldrich) were mixed in a molar ratio of 58.8: 41.2 with a total amount of 200 g and put inside a graphite crucible, which was transferred into the molten salt cell. The cell was placed inside a furnace equipped with a regulator and thermocouples (Eurotherm) refractory steel and closed by a stainless-steel lid cooled by circulating water. To remove residual moisture and oxides, the molten salt cell was initially dehydrated by heating under a vacuum (9×10^{-1} bar) to its melting point followed by protection of the Ar atmosphere.

Preparation of Ti_2AlC MAX Phase: To prepare the Ti_2AlC MAX phase, Ti (99% pure, Sigma Aldrich), Al (99.9% pure, 325 mesh), and C elemental powders were ground well according to a specific ratio (e.g., Ti:Al:C = 2:1.2:1 in molar ratio) and pressed into a pellet ($\Phi = 8$ mm) by a load of 4 ton. Three different forms of C were applied here including graphite (Sigma Aldrich), 1D few-walled CNT (Sigma Aldrich), and 2D rGO (Sigma Aldrich) prepared from Hummer's method, containing C, O, and H elements. The pellet was covered by Mo meshes to ensure electrical contact. In the next step, the pellet covered by Mo mesh was inserted inside the molten salt cell at 1000 °C for 1 h (graphite based), 970 °C for 50 min (CNT-based), and 950 °C for 1 h (rGO-based). The as-synthesized product was taken out and washed with deionized water via filtration, followed by drying inside an oven at 60 °C.

Preparation of E-Ti_2CT_x: To prepare the E-Ti_2CT_x MXene phase, the elemental pellet (Ti:Al:C = 2:1.2:1 in molar ratio) was inserted inside the molten salt cell and heated at 950 °C for 1 h (rGO-based) or 970 °C for 50 min (CNT-based). In the next step, the molten salt cell was cooled down to 500 °C and connected to the Autolab PGSTAT 30 potentiostat for further electrolysis experiment at a constant potential. During the electrolysis step, the above elemental precursors' pellet covered by Mo mesh was served as a working electrode and a graphite crucible used as a counter electrode (see Figure 1a). The electrolysis was done using a three-electrode cell set-up, the counter electrode was connected to the crucible and a glassy carbon electrode immersed in the molten electrolyte was used as a quasi-reference electrode. The electrolysis experiment was conducted by applying a constant voltage of 0.8 V (rGO-based) or 1.3 V (CNT-based) for 24 h to ensure all the Al atoms were selectively oxidized (the voltammeter in Figure 1a, to measure the voltage between working and counter electrode, which was around 2 V). The as-synthesized product was taken out and washed with deionized water via filtration, followed by drying inside an oven at 60 °C. The dried E-Ti_2CCl_x was treated in 0.02 M APS for 3 h or 0.1 M $FeCl_3$ for 2 h for further electrochemical study.

Physical Characterizations: XRD data were collected by a D4 X-ray diffractometer (Bruker, Germany) equipped with Cu$K\alpha$ radiation ($\lambda = 0.154$ nm). The morphology of the MXenes was observed with SEM JSM 7100F (JEOL, Japan) with energy-dispersive X-ray spectroscopy (EDX) capabilities. TEM and HRTEM images were performed using a JEOL ARM200F microscope equipped with a cold field-emission gun working at an acceleration voltage of 200 kV. Samples for cross-sectional TEM were prepared by an FEI-HELIOS 600i FIB system. HAADF-STEM images were collected with an angular collection semi-angle range from 50 to 180 mrad. A dispersion of 0.25 eV/channel was used for EELS. FTIR, in conjunction with attenuated total reflection, was used to record infrared spectra in a Thermo Scientific Nicolet model 6700 FT-IR spectrometer between 4000 and 400 cm^{-1}.

Electrochemical Measurements: E-Ti_2CT_x powders were mixed with PTFE binder and carbon black conducting additive (80 wt% of MXenes powders, 15 wt% of carbon black, and 5 wt% of PTFE binder) and calendered into the film. These as-prepared MXene electrode films were then dried in a vacuum oven at 80 °C for at least 10 h. After that, MXene films were used as the working electrode to assemble standard half-cells with metallic lithium foil as both the counter and reference electrode. The mass loading was controlled at ≈1.5 mg cm^{-2} with a Cu disk as a current collector. Commercial LP30 (1 M $LiPF_6$ in ethylene carbonate/dimethyl carbonate with a 1:1 volume ratio) was used as the electrolyte, while two layers of 260 µm-thick porous borosilicate glass fibers (Whatman GF/B) were used as the separator. Two-electrode Swagelok cells were assembled in an argon-filled glove box with oxygen and water content <0.1 ppm. Cyclic voltammetry and galvanostatic cycling were performed using a VMP3 potentiostat (Biologic, France) within a potential range from 0.01 to 3 V versus Li^+/Li. EIS was carried out in a two-electrode cell configuration. EIS measurements were performed at various biased voltages with a 10 mV amplitude between 10 mHz and 200 kHz. Before each EIS measurement, linear sweep voltammetry with a scan rate of 1 mV s^{-1} was applied to reach the desired voltage and followed by holding at the specific voltage for 10 min.

Supporting Information

Supporting Information is available from the Wiley Online Library or from the author.

Acknowledgements

L.L. was supported by ERC Synergy Grant MoMa-Stor#951513. P.S. and P.-L.T. acknowledge the support from Agence Nationale de la Recherche (Labex Store-ex) and ERC Synergy Grant MoMa-Stor #951513.

Conflict of Interest

The authors declare no conflict of interest.

Data Availability Statement

The data that support the findings of this study are available from the corresponding author upon reasonable request.

Keywords

electrochemical etching, Li-ion batteries, MAX, molten salts approach, MXenes

Received: November 9, 2022
Revised: December 5, 2022
Published online: December 30, 2022

[1] B. Anasori, M. R. Lukatskaya, Y. Gogotsi, *Nat. Rev. Mater.* **2017**, *2*, 16098.
[2] M. Ghidiu, M. R. Lukatskaya, M.-Q. Zhao, Y. Gogotsi, M. W. Barsoum, *Nature* **2014**, *516*, 78.
[3] M. R. Lukatskaya, S. Kota, Z. Lin, M.-Q. Zhao, N. Shpigel, M. D. Levi, J. Halim, P.-L. Taberna, M. W. Barsoum, P. Simon, *Nat. Energy* **2017**, *2*, 17105.
[4] L. Liu, P.-L. Taberna, B. Dunn, P. Simon, *ACS Energy Lett.* **2021**, *6*, 4311.
[5] M. Naguib, M. Kurtoglu, V. Presser, J. Lu, J. Niu, M. Heon, L. Hultman, Y. Gogotsi, M. W. Barsoum, *Adv. Mater.* **2011**, *23*, 4248.
[6] L. Liu, M. Orbay, S. Luo, S. Duluard, H. Shao, J. Harmel, P. Rozier, P.-L. Taberna, P. Simon, *ACS Nano* **2021**, *16*, 111.

[7] Y. Li, H. Shao, Z. Lin, J. Lu, L. Liu, B. Duployer, P. O. Persson, P. Eklund, L. Hultman, M. Li, *Nat. Mater.* **2020**, *19*, 894.
[8] G. Ma, H. Shao, J. Xu, Y. Liu, Q. Huang, P.-L. Taberna, P. Simon, Z. Lin, *Nat. Commun.* **2021**, *12*, 5085.
[9] M. Shen, W. Jiang, K. Liang, S. Zhao, R. Tang, L. Zhang, J. Q. Wang, *Angew. Chem.* **2021**, *133*, 27219.
[10] J. Xuan, Z. Wang, Y. Chen, D. Liang, L. Cheng, X. Yang, Z. Liu, R. Ma, T. Sasaki, F. Geng, *Angew. Chem.* **2016**, *128*, 14789.
[11] J. Chen, M. Chen, W. Zhou, X. Xu, B. Liu, W. Zhang, C. Wong, *ACS Nano* **2022**, *16*, 2461.
[12] W. Sun, S. Shah, Y. Chen, Z. Tan, H. Gao, T. Habib, M. Radovic, M. Green, *J. Mater. Chem. A* **2017**, *5*, 21663.
[13] M. Alhabeb, K. Maleski, B. Anasori, P. Lelyukh, L. Clark, S. Sin, Y. Gogotsi, *Chem. Mater.* **2017**, *29*, 7633.
[14] C. E. Shuck, M. Han, K. Maleski, K. Hantanasirisakul, S. J. Kim, J. Choi, W. E. Reil, Y. Gogotsi, *ACS Appl. Nano Mater.* **2019**, *2*, 3368.
[15] H. Shao, S. Luo, A. Descamps-Mandine, K. Ge, Z. Lin, P. L. Taberna, Y. Gogotsi, P. Simon, *Adv. Sci.* **2022**, 2205509.
[16] B. Liang, Z. Dai, W. Zhang, Q. Li, D. Niu, Y. Zhang, M. Jiao, L. Yang, X. Guan, *J. Asian Ceram. Soc.* **2021**, *9*, 815.
[17] T. Galvin, N. Hyatt, W. Rainforth, I. Reaney, D. Shepherd, *J. Eur. Ceram. Soc.* **2018**, *38*, 4585.
[18] W. S. Wolbach, R. S. Lewis, E. Anders, *Science* **1985**, *230*, 167.
[19] L. Liu, Y.-C. Wu, P. Rozier, P.-L. Taberna, P. Simon, *Research* **2019**, *2019*, 6585686.
[20] J. Haemers, R. Gusmão, Z. Sofer, *Small Methods* **2020**, *4*, 1900780.
[21] M. Naguib, V. N. Mochalin, M. W. Barsoum, Y. Gogotsi, *Adv. Mater.* **2014**, *26*, 992.
[22] M. R. Lukatskaya, J. Halim, B. Dyatkin, M. Naguib, Y. S. Buranova, M. W. Barsoum, Y. Gogotsi, *Angew. Chem.* **2014**, *126*, 4977.
[23] C. Torres, R. Quispe, N. Z. Calderón, L. Eggert, M. Hopfeld, C. Rojas, M. K. Camargo, A. Bund, P. Schaaf, R. Grieseler, *Appl. Surf. Sci.* **2021**, *537*, 147864.
[24] P. Zhang, Z. Li, S. Zhang, G. Shao, *Energy Environ. Mater.* **2018**, *1*, 5.
[25] R. Arenal, K. March, C. P. Ewels, X. Rocquefelte, M. Kociak, A. Loiseau, O. Stéphan, *Nano Lett.* **2014**, *14*, 5509.
[26] P. Lindgren, L. Hallis, F. S. Hage, M. R. Lee, J. Parnell, A. Plan, A. Doye, I. MacLaren, *Meteorit. Planet. Sci.* **2019**, *54*, 2698.
[27] P. Liu, B. Guan, M. Lu, H. Wang, Z. Lin, *Electrochem. Commun.* **2022**, *136*, 107236.
[28] K. Brezesinski, J. Wang, J. Haetge, C. Reitz, S. O. Steinmueller, S. H. Tolbert, B. M. Smarsly, B. Dunn, T. Brezesinski, *J. Am. Chem. Soc.* **2010**, *132*, 6982.
[29] V. Augustyn, J. Come, M. A. Lowe, J. W. Kim, P.-L. Taberna, S. H. Tolbert, H. D. Abruña, P. Simon, B. Dunn, *Nat. Mater.* **2013**, *12*, 518.
[30] A. N. Banerjee, V. Anitha, S. W. Joo, *Sci. Rep.* **2017**, *7*, 13227.
[31] O. Okhay, A. Tkach, *Nanomaterials* **2021**, *11*, 1240.
[32] Y. Xie, M. Naguib, V. N. Mochalin, M. W. Barsoum, Y. Gogotsi, X. Yu, K.-W. Nam, X.-Q. Yang, A. I. Kolesnikov, P. R. Kent, *J. Am. Chem. Soc.* **2014**, *136*, 6385.
[33] Y. Wang, C. Ma, W. Ma, W. Fan, Y. Sun, H. Yin, X. Shi, X. Liu, Y. Ding, *2D Mater.* **2019**, *6*, 045025.
[34] S. Kajiyama, L. Szabova, H. Iinuma, A. Sugahara, K. Gotoh, K. Sodeyama, Y. Tateyama, M. Okubo, A. Yamada, *Adv. Energy Mater.* **2017**, *7*, 1601873.